Paper accepted by Vehicle System Dynamics, doi: 10.1080/00423114.2021.1928248

Vibration Reduction of a High-Speed Train Floor using Multiple Dynamic Vibration Absorbers

Taiwen YOU[1] Jinsong ZHOU[1] David J Thompson[2] Dao GONG[1]* Jiangxue Chen[1] Yu Sun[1]

(1, Institute of Rail and Transit, Tongji University, No. 4800, Cao an Road, Shanghai 201804, People's Republic of China

2, Institute of Sound and Vibration Research, University of Southampton, Southampton, UK)

**Corresponding author: gongdao@tongji.edu.cn*

Abstract: Due to local resonances, high vibration levels of the floor occur frequently in high-speed trains, which have a great negative impact on the ride comfort. A method is presented to control excessive local vibration of the internal floor of a high-speed electric multiple unit train by using multiple dynamic vibration absorbers (DVAs). The possible causes of the high vibration levels of the internal floor are investigated using operational and modal tests. To reduce the vibration, a model of the vehicle body with multiple DVAs is established based on the modal superposition method. The contribution of different modes at the dominant vibration peaks is assessed and targeted. It is found that a strong peak at around 12 Hz is dominated by a single mode, which can be attenuated by using a single DVA, which can be applied outside the car body, such as under-frame equipment. In the frequency region between 30 and 35 Hz several local modes contribute, and can be controlled by using multiple DVAs. Methods are studied to determine the optimal parameters for these DVAs, including location, natural frequency and mass. For a single DVA conventional fixed-point theory is used, whereas for multiple absorbers an optimization method is proposed. Finally, the effect of applying DVA solution is verified in the full vehicle model using frequency responses analysis. The results indicate that the proposed method can effectively reduce the vibration of targeted modes and improve the ride quality considerably in terms of the vertical motion.

Key words: High-speed EMU trains; Floor vibration; Dynamic vibration absorber; Modal contribution

1 Introduction

The increment of operational speeds of high-speed electric multiple unit (EMU) trains and their lightweight design result in intense excitation to vehicle systems and more significant vibration. The interior floor, an important component in EMU, is usually resiliently mounted from the main car body structure. It covers a large area inside the vehicle with lower elastic modulus than car body. Consequently, if the floor structure is not properly designed, it will generate large vibration levels and adversely affect the passenger's feeling. According to the relevant standards in Europe and China, the response at the floor is usually taken as the input for ride comfort evaluation [1,2]. Therefore, it is critical to control the vibration of the internal floor for improving passenger's feeling. Unfortunately, once the floor is installed it is very difficult to rectify any problems that arise.

Most previous researches are focused on the analysis and reduction of the overall vehicle body vibration [3-6], including vibration occurred by the lozenging deformation mode, first-order vertical bending mode, torsional modes, etc. To investigate the influence from lightweight design on vehicle dynamics, Zhou et al. [7] built a model of the vertical vibration of railway passenger vehicles, including the first mode of car body verified with actual experiments and all vertical rigid modes. The results showed that when the stiffness of the carbody is reduced beyond a certain amount, there can be a significant reduction in the natural frequencies of the carbody. Foo and Goodall [8] proposed a proportional integral (PI) control method to suppress vertical flexural vibration of a railway vehicle car body, which was validated in a 1D vehicle dynamics simulation model and established as a simple uniform Euler–Bernoulli beam supported on the secondary suspensions, in which only vertical vibration modes of the carbody, i.e. bounce, pitch, and flexible bending modes, were considered. Carlbom [9] investigated the vibration of carbody in the multi-body system dynamic simulation and established a non-linear multi-body model with a finite element model of the carbody. Gong et al. [10] constructed a rigid-flexible coupled dynamic model of a carbody, which adopted the Craig-Bampton condensation method in FEM software and verified with an actual modal experiment.

Some research also refers to the local vibration of carbody. Tomioka et al. [11] presented an analytical method to investigate the vibration of the carbody modelled as a box-type structure consisting of plates and beams. And verified this model with an experiment model. Wang et al. [12] simplified the floor as a rectangular plate stiffened by beams in two orthogonal directions, while vertical motion and rotation of the plate–column joints are viewed as the unknown degrees of freedom.

However, in the studies discussed above, the interior trim was neglected in the car model or only considered as a part of the overall body. Models in existing research are therefore not able to study the local vibration problems of the interior trim of high-speed trains such as floors, seats, luggage, etc. occurs frequently [4,6]. Moreover, yet few studies have been reported on the vibration controlling of an EMU floor. The methods of vibration controlling applied to train floors are mostly empirical, such as modifying the location and extent of the support structure between the inner floor and the structural floor [4,10-14], or using high-damping material [14]. Hudson et al. [15] performed a multiple objective optimization to minimize the mass and cost of composite sandwich panels for the interior floor

structure of a metro car. Takigami et al. [16] designed a rigidity test to study the influence of non-structural members in the car body on its rigidity and vibration. However, once a vehicle has been put into operation, modification of the vehicle structure would cause great additional costs, and the safety of the vehicle cannot be guaranteed after that modification.

Dynamic vibration absorbers (DVAs) provide another solution for reducing the vibration of structures. These consist of damped mass-spring systems tuned to match the natural frequencies of the host structure. Den Hartog [20,21] proposed the 'fixed-point theory' and gave a simple design relationship for identifying optimal parameters. This method has been widely adopted in structural vibration control. Nguyen et al. [22] configured multiple DVAs (referred to as tuned mass dampers) to control floor vibration. The installed DVAs reduced the floor vibration by at least 40%.

Recently, the application of DVAs has been considered for various applications in the field of railway vibration. Zhu et al. [23] shown a DVA application controlling the low-frequency vibration of floating slab tracks. Collette et al. [24] presented a DVA applied to a wheelset to mitigate rutting corrugation of the rail. Chen et al. [25] considered the performance of DVAs applied to a bridge in suppressing the response to earthquake loading. Gong et al. [26] used under-frame equipment as a DVA to reduce the first vertical bending mode of the vehicle body.

The aim of the present paper is to use multiple DVAs reducing the low frequency local vibration of the interior floor in a high-speed EMU train. The main cause of local resonances is first investigated with transmissibility measurements and a modal test of floor. An improved numerical model consisting of the floor, carbody and multiple DVAs is proposed and used to determine the transmissibility. The transmissibility was used to compute the optimal parameters of each DVA, and a contribution analysis was conducted to determine the most contribution mode to the response. Finally, the optimized parameters are introduced into the simulation model to evaluate the performance of the proposed DVAs in the frequency domain and the effect on the ride comfort index.

2 Experimental investigation of local vibration of the floor

2.1 Operational measurements of floor vibration

Some passengers complain about dizziness or an unexplained foot numbness, especially when sitting near the middle of the carbody. To investigate this, operational tests were conducted to measure floor vibration in service. When passengers are exposed to an intensive vibration environment, a critical vibration frequency range between 0.5 and 80 Hz, generally regarded as having significant effects on the human body, especially the vibration at 5-30 Hz causes resonance in the head. During these tests, accelerometers were arranged to measure the vertical vibration with the sampling frequency of 1024 Hz, at standard positions according to UIC 513 [1] including the floor above the front bogie, in the middle of the vehicle and above the rear bogie. Here the lowest sampling frequency should meet the requirements of Nyquist sampling law and the digital feeling filter for the calculation of ride comfort index. The point above the bogie must be positioned above the centre of the left and right air springs and the point in the centre of the body must be mounted in the middle of the interior passageway. All accelerometers were arranged with the same altitude on the floor and should be moved in the same way as the moving part of the same structure as the seat. It must be ensured that the connectivity of the accelerometer and the fixed points are as rigid as possible. What's

more, the acceleration from air springs is also collected with the sampling frequency of 1024 Hz to analyse the vibration in the simulation mode. For input signal collected, accelerometers were arranged next to the air springs.

Fig. 1(a) shows the measured vibration spectrum of the floor at the three sensor locations. The vibration amplitude at the centre of the floor is significantly higher than at the other positions, especially below 20 Hz. In particular, strong peaks occur at around 12 Hz and 33 Hz. According to the frequency weighting curve in the UIC513 standard [1], the vertical vibration has the highest weighting in the frequency range 4-20 Hz. Therefore, the high vibration amplitude at 12 Hz around the middle of the floor will greatly affect the ride comfort. Moreover, the 30-40 Hz band also falls within the human body's sensitive frequency band [27]. Therefore, a modal test of the floor and carbody was carried out to analyse the cause of these peaks.

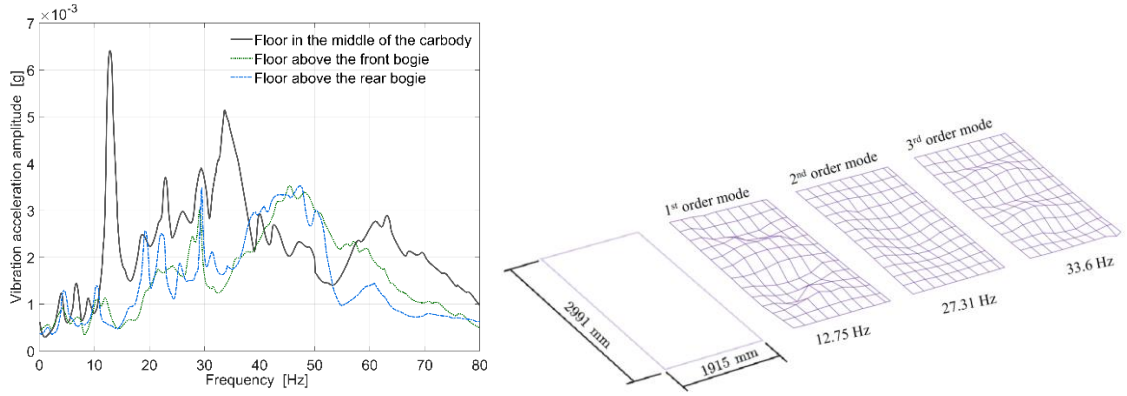

(a) (b)

Fig. 1 Measured results: (a) vertical vibration acceleration spectrum at ride quality testing points at 350 km/h; (b) The first three modes measured on the interior floor.

2.2 Modal test of floor

A single-input-single-output modal test method [28] is used to identify the natural frequencies and mode shapes of the internal floor. On the floor surface, 13 sections are selected at equal intervals of 250 mm along the length direction near the centre of the vehicle. 10 points are equally spaced across the width on each section as the vertical excitation point of the hammer. The centre point of the floor is selected as the output point at which the accelerometers is attached. During the measurement, the weight of the used hammer is 0.72 kg and the sampling frequency is set to 1024 Hz. The frequency response around 0-50 Hz at the centre of the interior floor is collected from impact excitation at various points while the vehicle is stationary. The first three measured modes of the floor are shown in Fig. 1(b).

As can be seen, the first modal frequency of the floor is 12.75 Hz, according to the modal test results of the whole car body, this mode corresponds to the first order vertical bending mode of the whole car body. The frequencies of the first and third modes are close to the peaks in Fig. 1.

The interior floor is made of a composite material, and its elastic modulus is smaller than vehicle's without the local vibration problem. Because of the low vertical stiffness, the internal floor supported on a large number of discrete mounts, between 500 and 700, to provide local stiffness. The natural frequency of the floor on its mounts is intended to be above 50 Hz. However, due to the poor distribution of mounts, there can be locations that have insufficient support, resulting in local vibration.

3 Model of floor vibration with multiple dynamic vibration absorbers

Recently, FEA has been adopted with the pseudo-excitation method [29] to obtain the vibration at a precise point, but the results depend on the element size, number of master nodes selection in the condensation process and the error of condensation method. A method is introduced to obtain the vibration at an arbitrary location with excitation coming from a vehicle system dynamics model or from measurement. As shown schematically in Fig. 2, the vehicle consists of the carbody, structural floor, interior floor and isolation mounts. The interior floor is treated as a rectangular plate supported by mounts above the structural floor. The carbody including the structural floor and interior floor can be modelled with finite elements or an analytical method. In order to control the vibration in certain locations, a number of DVAs are installed on the floor, as shown in Fig. 2.

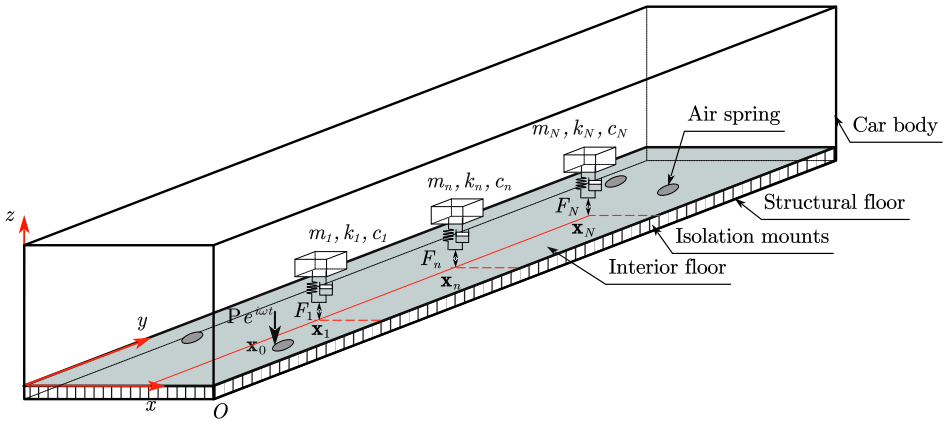

Fig. 2 Representation of the theoretical model of vehicle floor vibration including multiple dynamic vibration absorbers

The vibration of the interior floor can be treated as a plate with force excited at the secondary suspension air springs. N DVAs are attached to the interior floor. In deriving the equation of motion for the combined system, including added DVAs, the coordinates shown in Fig. 2 are used and the deflection amplitudes of the host structure and the DVAs are denoted by $\mathbf{W}=[W_1\ W_2\ \ldots\ W_m]^T$ and $\mathbf{Z}=[Z_1\ Z_2\ \ldots\ Z_n]^T$, respectively. As the modal and operation experiment result demonstrate that the local resonance often occurs at a certain frequency, an external harmonic point force with amplitude P and circular frequency ω is applied at a general position $\mathbf{x}_0$. The equations of motion for the system in the frequency domain can be expressed as

$$(-\omega^2\mathbf{M}_c + i\omega\,\mathbf{C}_c + \mathbf{K}_c)\,\mathbf{W} = \mathbf{P} - \mathbf{F} \tag{1}$$

where $\mathbf{M}_c$, $\mathbf{K}_c$ and $\mathbf{C}_c$ are the mass, stiffness and damping matrices of the main body. m is the number of the nodes of the FE model in carbody; $\mathbf{P}=[P_1\ P_2 \ldots P_m]^T$ is the external force vector including force from the second springs, bumps et al. when $\mathbf{x}=\mathbf{x}_0$, $P_m=P$, otherwise $P_m=0$; $\mathbf{F}=[F_1\ F_2 \ldots F_m]^T$ is the reaction force from the DVAs which is an interior force and when $\mathbf{x}=\mathbf{x}_n$, $F_m=F_n$, otherwise $F_m=0$. The reaction force F_n applied by the n-th DVA at the location $\mathbf{x}_n$ is given by

$$F_n = k_n\,(W_n - Z_n) + i\omega\,c_n\left(\dot{W}_n - \dot{Z}_n\right) \tag{2}$$

in which k_n and c_n are the spring stiffness and dashpot damping of the connecting springs and dampers between the

main structure and the *n*-th DVA.

To obtain the solution of Eq. (1), it is usually used that supposing the solution is a form of harmonic response, which needs the inverse of a matrix. Fortunately, the modal expansion method [30] provides a solution while avoiding working with large matrices. The normalized eigen-function the main structure is denoted by $\mathbf{\Phi}(\mathbf{x})$ and the mass, stiffness and damping matrix will be normalized in modal coordinates. The following approximate expressions can be used for the solution of Eq. (1):

$$\mathbf{W} = \sum_{j=1}^{J} \boldsymbol{\Phi}^{j}(\mathbf{x})\mathbf{u}^{j} = \mathbf{\Phi}(\mathbf{x})\mathbf{U} \tag{3}$$

$$\begin{aligned} &\mathbf{\Phi}(\mathbf{x}) = [\boldsymbol{\Phi}^{1}(\mathbf{x})\ \boldsymbol{\Phi}^{2}(\mathbf{x})\ \cdots\ \boldsymbol{\Phi}^{J}(\mathbf{x})]^{T} \\ &\mathbf{U} = [\mathbf{u}^{1}\ \mathbf{u}^{2}\ \cdots\ \mathbf{u}^{J}]^{T} \end{aligned} \tag{4}$$

in which $\mathbf{U}$ is the generalised coordinate of the main body and the approximation is due to the truncation of the sum at J. Here the modal coordinates depend on the initial and boundary condition, in this study it's a form of harmonic formula at each node. The truncation is limited by the frequency focused on.

Substitution of Eq. (3) into Eq. (1), and rearrangement according to orthogonality of the eigen-functions, leads to a differential equation:

$$(-\omega^{2}\mathbf{M} + i\omega\mathbf{C} + \mathbf{K})\mathbf{Q} = \mathbf{\Gamma} \tag{5}$$

where the mass, damping and stiffness matrices in Eq. (5) are given by

$$\begin{aligned} \mathbf{M} &= \begin{bmatrix} [M_d] & & 0 \\ & m_1 & \\ 0 & & \ddots \\ & & & m_N \end{bmatrix} \\ \mathbf{C} &= \begin{bmatrix} [C_d] + \sum_{n=1}^{N} c_n \mathbf{\Phi}(\mathbf{x}_n)\mathbf{\Phi}(\mathbf{x}_n)^{T} & -c_1\mathbf{\Phi}(\mathbf{x}_1) & \cdots & -c_n\mathbf{\Phi}(\mathbf{x}_n) \\ -c_1\mathbf{\Phi}(\mathbf{x}_1) & c_1 & & \\ \vdots & & c_2 & \\ -c_n\mathbf{\Phi}(\mathbf{x}_n) & & & c_n \end{bmatrix} \\ \mathbf{K} &= \begin{bmatrix} [K_d] + \sum_{n=1}^{N} k_n \mathbf{\Phi}(\mathbf{x}_n)\mathbf{\Phi}(\mathbf{x}_n)^{T} & -k_1\mathbf{\Phi}(\mathbf{x}_1) & \cdots & -k_n\mathbf{\Phi}(\mathbf{x}_n) \\ -k_1\mathbf{\Phi}(\mathbf{x}_1) & k_1 & & \\ \vdots & & k_2 & \\ -k_n\mathbf{\Phi}(\mathbf{x}_n) & & & k_n \end{bmatrix} \end{aligned} \tag{6}$$

where $[\mathrm{M}_d] = \mathrm{diag}(M_1, M_2, \ldots, M_j)$ is the modal masses including the transformation mass from carbody, interior material and equipment, $[\mathrm{K}_d] = \mathrm{diag}(K_1, K_2, \ldots, K_j)$ contains the modal stiffness which depends on the type of material, and $[\mathrm{C}_d] = \mathrm{diag}(C_1, C_2, \ldots, C_j)$ is modal damping values and can be obtained from the insert loss of material.

$\mathbf{\Gamma}$ is the vector of the external force in generalised coordinates which can be expressed as:

$$\mathbf{\Gamma} = \begin{bmatrix} \mathbf{\Phi}(\mathbf{x}_0)^{T}\mathbf{P} \\ \{\mathbf{0}\}_{1*m-n} \end{bmatrix} \tag{7}$$

and the generalised displacement vector is given by

$$\mathbf{Q} = \begin{bmatrix} \mathbf{U} \\ \mathbf{Z} \end{bmatrix} \tag{8}$$

The displacement of the DVAs can be written as follows:

$$\mathbf{Z}(\omega) = [Z_1(\omega)\ Z_2(\omega)\ \cdots\ Z_N(\omega)]^T \tag{9}$$

4 Numerical simulation

4.1 Establishing and updating the simulation model

In order to demonstrate the method proposed for floor vibration control, a detailed finite element model of the tested EMU vehicle body was constructed in Optistruct. The isolation mounts between the interior floor and the car body structure, and the composite material floor are both included in this model. The model is shown in Fig. 3 and includes shell elements (CQUAD4) for the vehicle body and hexahedral(CHEXA) solid elements for the isolation mounts and interior floor. The main material parameters of each part are that the Young's modulus, Poisson's ratio and density of carbody are 69000 Mpa, 0.3 and 2700 kg/m3 respectively. The composite floor is established with an anisotropic material, in which Young's modulus, shear modulus in different directions is EX=EY=0.7, EZ=1600, GX=0.4, GY=250, GZ=110 and the density is 300 kg/m3. The finite element model contains 631,657 elements and 729,410 nodes.

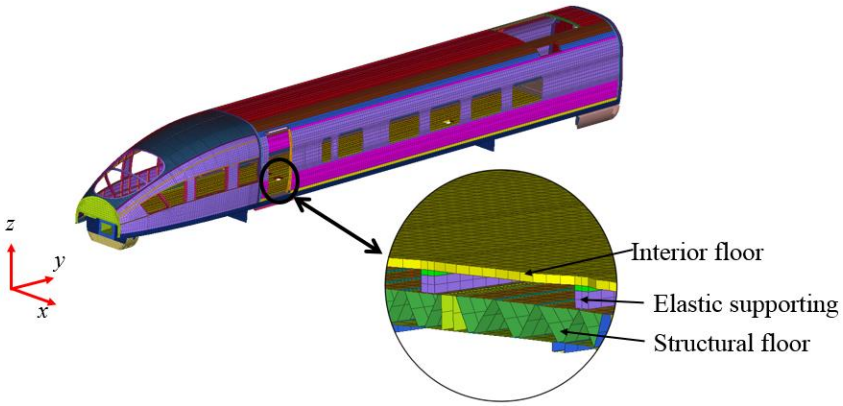

Fig. 3 The finite element model of carbody and floor

After the FEM establishment, it was calibrated by adjusting model parameters such as the thickness of shell elements, the elastic modulus and the material damping [29] to match the results of modal and operational tests. The final selected parameters are that the Young's modulus, Poisson's ratio, Structural damping coefficient and density of carbody are 73000 Mpa, 0.3, 0.004 and 2847 kg/m3 respectively and the thickness of structure floor was strengthened 1-3 mm averagely. In the present work, the frequency response at the centre of the interior floor due to impact excitation at various points was chosen to update the FEM model [31]. The first three natural frequencies of the car body after updating are compared with the measured results in Tab. 1. It can be seen that the finite element calculation results of the vehicle body are consistent with the experimental test results, with the maximum error of 2.5%. Moreover, the first-order vertical bending mode of the carbody is found at 12.75 Hz, which is a whole carbody

motion in vertical direction suggests that the vibration peak occurs by a mode of the whole structure rather than the internal floor.

Tab. 1 Modal test and simulation results of the car body

Mode shape	Simulation result	Test result	Error (%)
First-order vertical bending	12.53	12.75	1.8
First-order transverse bending	16.17	15.76	2.5
First order twisting	16.89	17.21	1.9

The first 40 Hz acceleration calculation results at the centre of the floor are compared in Fig. 4 with the measured spectrum from the operational test. It can be seen that the spectra show similar trends and features: both contain a strong peak at around 12 Hz; the amplitude of this peak is predicted within 7% of the measured value. This indicates that the FEM is acceptable under impact excitation at certain points and for a stationary vehicle.

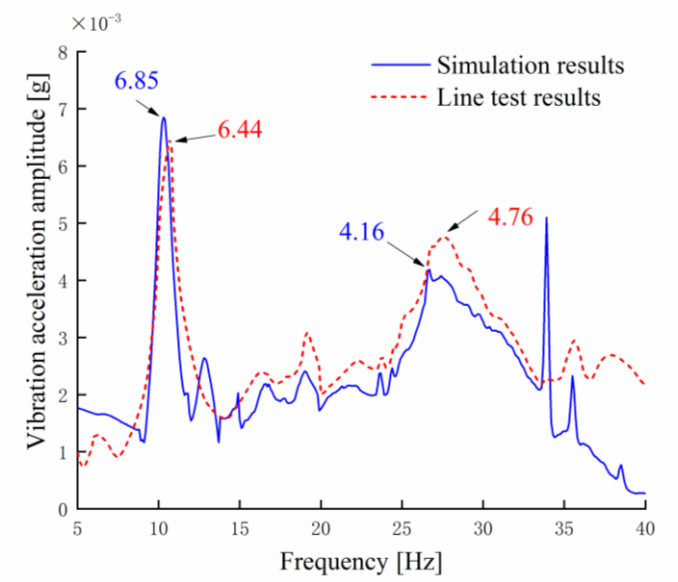

Fig. 4 Comparison of simulation results and operational test results of vibration acceleration at centre of interior floor

4.2 Determination of the target modes for floor vibration control

In section 2, the modal test results of the interior floor demonstrated that there are modes at 12.75 Hz and 35 Hz, close to the peaks in the vibration. But it should be pointed out that the peak of response is not rely on modes close to peaks merely, It's an accumulated result of all modes. When designing the DVAs, the role for different modes on peaks should be identified, some targeted modes are out phase with the response and should be strengthen not supressed. A modal contribution method is used for this. For the vibration model without DVAs, which is a proportionally damped system, the square damping matrix is diagonal and the vibration of the carbody can be expressed as:

$$(-\omega^2\mathbf{M}_c + i\omega\mathbf{C}_c + \mathbf{K}_c)\mathbf{W} = \mathbf{P} \tag{10}$$

Substituting the transformation of Eq.(3) into Eq.(10), each of the J uncoupled differential equations in Eq.(10) is of the form:

$$\mathrm{diag}\left[-\omega^2\bar{m}_j + i\omega\bar{c}_j + \bar{k}_j\right]\mathbf{U} = \mathbf{\Phi}^T\mathbf{P} \tag{11}$$

where $\bar{m}_j$ is the generalized mass of the j-th mode, $\bar{c}_j$ is the generalized damping and $\bar{k}_j$ is the generalized stiffness.

From Eq.(11), the vibration of single mode satisfies

$$\left(-\omega^2\bar{m}_j+i\omega\bar{c}_j+\bar{k}_j\right)Q_j=\boldsymbol{\varphi}_j^T\mathbf{P} \tag{12}$$

where Q_j is the amplitude of the *j*-th mode.

For the given external dynamic forces defined by **P**, the dynamic response of a multi-degree-of-freedom system in frequency domain can be determined by solving Eq.(12). Thus, the *j*-th modal contribution factor [32] can be determined as follows:

$$Q_j=\frac{\boldsymbol{\varphi}_j^T\mathbf{P}}{-\omega^2\bar{m}_j+i\omega\bar{c}_j+\bar{k}_j} \tag{13}$$

This factor can identify modes that mostly contributed the response and search modes close to the peak, when closely spaced modes are present.

By using Eq. (13), the contributions of different modes in the response at 12 Hz and 33.6 Hz were identified in Fig. 5. The corresponding mode shapes of the internal floor are also shown. The first-order mode of the interior floor, which actually is a part of the first-order vertical bending mode of the carbody, with 93.2% contribution at 12 Hz. The peak at 33 Hz is mainly dominated by the modes at 33.6 Hz and 38.2 Hz, with contributions of 77.3% and 54.0%, respectively. It is noteworthy that some modes, such as the mode at 41.7 Hz, provide a negative contribution in the graph as their response is out of phase with the main modes.

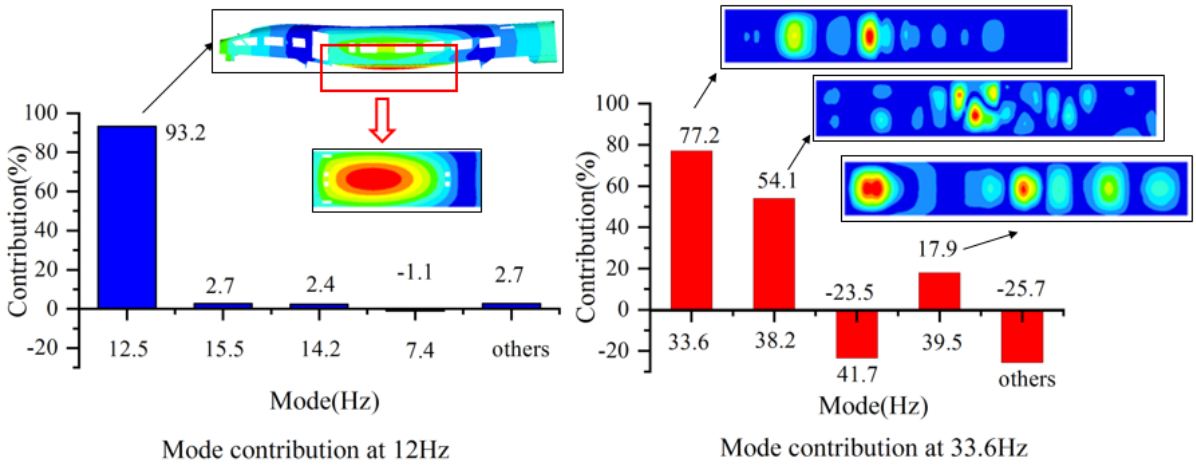

Fig. 5 The contribution of different modes at 12 Hz and 33.6 Hz

From the calculation results, the following conclusions are determined: (1) The first-order vertical bending is the main contributor to the vertical vibration in the middle part of the carbody and the mode observed on the floor at 12.5 Hz is part of the first-order vertical bending mode of the carbody. (2) These modes have large amplitudes on the interior floor at 33.6 and 38.2 Hz are the main cause of the peak found at 33Hz.

Based on the above analysis the target modes for the vibration control of different peaks are determined. The vibration of the floor near 12 Hz caused by only a single mode, a single dynamic vibration absorber will be sufficient to control this vibration. while the vibration response near 33 Hz comes mainly from two modes, multiple DVAs will be applied to reduce vibration from multiple modes.

4.3 Optimization of the distributed DVAs

For controlling the vibration occurred by a single mode, the fixed-point theory is a convenient and mature method. But for multiple DVAs application, this theory is not suitable. The above discussion shows the possibility of using DVAs to control the vibration of the interior floor and the target modes have been determined. The performance of DVAs installed in a structure depends on the ratio between the total mass of the DVAs and the mass of the structure, damping ratio, and the location of the DVAs. All these parameters should be designed carefully for controlling the local vibration. This section will discuss the design method for selecting suitable parameters of the DVAs.

When designing parameters of the DVA, the transmissibility, transmittance function and the PSD can be used. The transmittance function is the ratio of output response to input force, however, the input force cannot be obtained in the measurement. For the PSD, it is required to calculate the transfer function under random excitation [18], i.e. the output self-spectrum divided by the cross spectrum between the input and output location, which is a complex calculation process involving multiple integrations and is not convenient for engineering applications. For the vibration transmissibility, it is the amplitude ratio of output acceleration to input signal, only depends on the structure property and can be obtained easily from the measurement and simulation results. Therefore, in this work the vibration transmissibility is applied and the corresponding derivation was presented in Appendix A. The transmissibility of acceleration and input signal under the *j*-th mode is:

$$T = \sqrt{\frac{\varphi_j(\mathbf{x}_0)^2 \omega_j^4 (\lambda_j^2)^2 [(\gamma^2 - \lambda_j^2)^2 + (2\zeta\lambda_j)^2]}{[(1-\lambda_j^2)(\gamma^2 - \lambda_j^2) - A\gamma^2\lambda_j^2]^2 + [1-(1+A)^2\lambda_j^2]^2 (2\zeta\lambda_j)^2}} \tag{14}$$

Using the fixed-point theory [20], the optimal tuned-frequency ratio is given by

$$\gamma_{op} = \frac{1}{1+A} \tag{15}$$

and the optimal damping ratio of the distributed DVAs is

$$\zeta_{op} = \sqrt{\frac{3A}{8(1+A)^3}} \tag{16}$$

5 Verification of DVA

5.1 A single DVA to control floor vibration

As the vibration around 12 Hz is dominated by a single mode of the vehicle body, a single dynamic vibration absorber is adopted to control this mode. The system shown in Fig. 2 can be treated as a two-degree-of-freedom system in Fig. 6, where the meaning of all the parameters can be found in Eq. (A10).

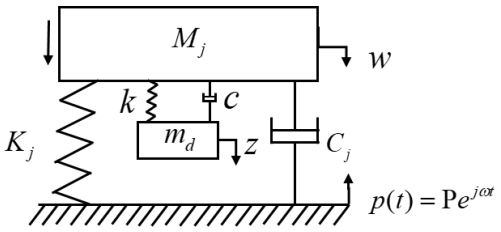

Fig. 6 Schematic diagram of two-degree-of-freedom system including vibration absorber

Using Eq. (15) and (16), the optimal parameters of a single DVA can be directly obtained. Here, the 12.5 Hz mode is targeted, and the corresponding modal mass can be obtained by the equivalent mass identification method [20]. The parameters of a single DVA calculated by the above method are μ = 0.01-0.1, λ = 0.95, ζ = 0.071-0.09 (depending on the mass).

To verify this method, the DVA is established in the FEM model by introducing 1D spring element (CELAS1) representing the stiffness part in the DVA, 1D mass element representing mass of absorber and 1D bush element (CBUSH 1D) is introduced as damper. Each part is connected to the carbody with node interaction. The simulation results with single DVA are shown in Fig. 7. The transmissibility, shown in Fig. 7(a), reduces in the region around 10-15 Hz with the growth of the mass ratio. The smallest value found is about 0.4 when the mass ratio is 0.1; here, the mass of the DVA is 830 kg. The transmissibility at other frequencies is not affected much. For the response of floor to the measured input, shown in Fig. 7(b), a similar trend is seen. Moreover, the mode at around 12 Hz will be substituted by two new modes which can be found in the Fig.7 (a). There are two peaks occur on the curve when the damping ratio is 0.1, one of the mode is generated by the DVA and the movement is mainly focused on the DVA, the other one is the influenced vertical bending mode with a higher frequency than the carbody without DVA.

Since the targeted mode is the vertical bending mode of the vehicle body, the mass identified for the DVA seems too large to install on the interior floor. A feasible method is to treat the under-frame equipment such as the traction transformer, and air compressor can be treated as the heavy mass DVA as a heavy mass DVA to decrease the influence of the first vertical bending mode [27], which in turn can control the local vibration in the middle of the interior floor at this frequency.

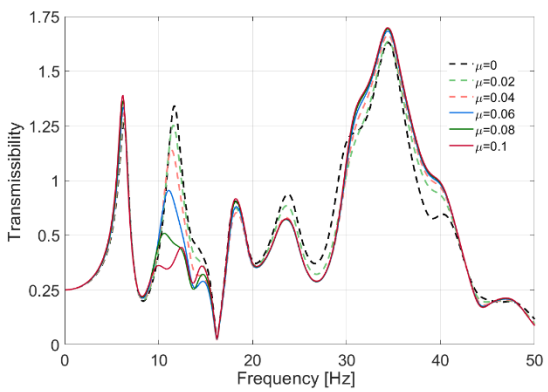

(a) Transmissibility of point at the middle of floor

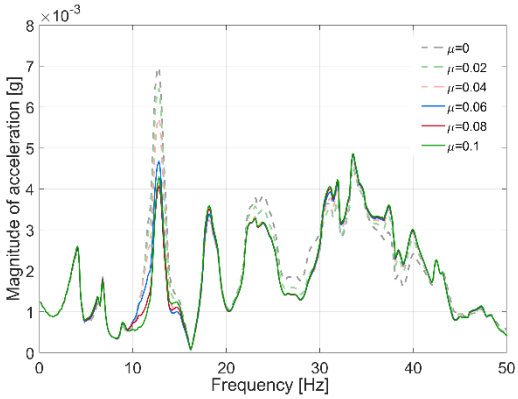

(b) Acceleration spectra of point at the middle of floor

Fig. 7 The influence of dynamic vibration absorbers with different mass ratios on vibration acceleration and transmissibility of floor

$$(\mu_o = 0-0.1, \gamma_o = 0.7, \zeta_o = 0.0122-0.369)$$

5.2 Multiple DVAs to control floor vibration

For the frequency band 30-40 Hz, multiple modes contribute to the response and multiple dynamic vibration absorbers (MDVAs) are necessary to control the vibration. The design of the MDVAs is different from the design of single DVA, an optimization method is proposed to find the suitable parameters of each DVA.

The objective function used to evaluate the effectiveness of the MDVAs is the average value of the amplitude of each frequency within the considered bandwidth from 30 Hz to 40 Hz. The design variables including stiffness and damping ratio considered as discrete variables, as well as the position of the MDVAs on the structure. Thus, the optimization problem is transformed into determining the optimum position and parameters of each DVA with minimizing the expected value [33]:

$$Minimizes\ J = E\left[\ddot{W}(A,\gamma,\omega,\ \mu,\zeta_d)\right]$$

$$subject\ to \begin{cases} \dfrac{\omega_{d,\min}}{\omega_j} \leqslant \gamma \leqslant \dfrac{\omega_{d,\max}}{\omega_j} \\ \dfrac{m_{d,\min}}{M_j} \leqslant \mu \leqslant \dfrac{m_{d,\max}}{M_j} \\ \dfrac{c_{d,\min}}{2m_{d,\min}\omega_{d,\min}} \leqslant \zeta_d \leqslant \dfrac{c_{d,\max}}{2m_{d,\max}\omega_{d,\max}} \\ 2\pi\times 30 \leqslant \omega \leqslant 2\pi\times 40 \end{cases} \tag{17}$$

5.2.1 Placement of DVAs

In Eq. (A.15), if the DVA is installed at different positions, the corresponding mode shape will change, which in turn affects the DVA controlling performance. Therefore, it is necessary to determine the optimal installation position before optimization of the other parameters.

In Eq. (A.12) the acceleration depends on two parts: the input signal and original property. For the placement of DVA, the modal shape value is the single relevant factor to the location. In modal space, the maximum value of mode shape is 1 and the minimum is 0. if the DVA is mounted at the maximum mode shape the Eq. (A.16) will be given by:

$$\lim_{\varphi(\mathbf{x}_n)\to 1} A = \mu \lim_{\varphi(\mathbf{x}_n)\to 1} \sum_{j=1}^{J} \varphi_j^2(\mathbf{x}_n) = \mu J \tag{18}$$

Supposing the variable in Eq. (A.12) is only the mounted location and other parameters are constant, the acceleration will only rely on the mode shape and the minimum value can be express as:

$$\left|\ddot{W}_j\right| = \frac{|\varphi_j(\mathbf{x}_0)|\omega_j^2}{\sqrt{\mathrm{Re}^2+\mathrm{Im}^2}} \tag{19}$$

where

$$\mathrm{Re} = 1-\frac{1}{\lambda_j^2} + \mu J \sum_{n=1}^{\mathrm{N}} \frac{\left[\left(1-\lambda_j^2/\gamma_{jn}^2\right)+\left(2\zeta_n\lambda_j/\gamma_{jn}\right)^2\right]}{\left(1-\lambda_j^2/\gamma_{jn}^2\right)^2+\left(2\zeta_n\lambda_j/\gamma_{jn}\right)^2} \tag{20}$$

$$\mathrm{Im} = \mu J^2 \sum_{n=1}^{N} \frac{(2\zeta_n \lambda_j^3/\gamma_{jn}^3)}{(1-\lambda_j^2/\gamma_{jn}^2)^2 + (2\zeta_n \lambda_j/\gamma_{jn})^2} \tag{21}$$

It can be seen from Eq.(19) that if the DVA is installed closed to the maximum mode shape, the magnitude of the acceleration will get the minimum value. Therefore, each DVA should be placed more close to the maximum mode shape. To demonstrate the influence of the location, a single DVA is introduced at various locations in FEM to control the mode at 33.6 Hz. As shown in Fig. 8 (a), the absorbers are arranged at positions from the input point to the maximum mode shape, at intervals of 1/4 of distance *L*. The output point at the centre of the floor is close to the position identified as 3/4 *L*.

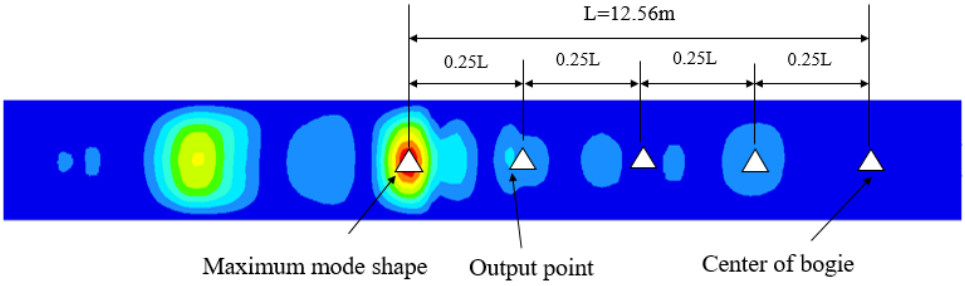

(a)

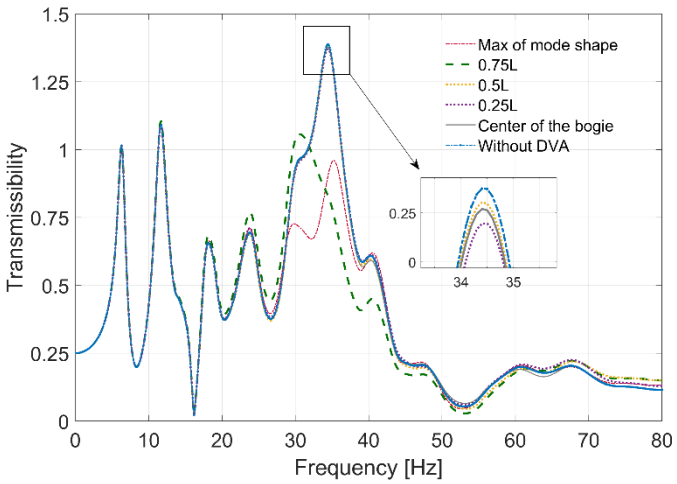

(b)

Fig. 8 (a) Schematic diagram of installing dynamic vibration absorbers in different positions
(b) The vibration acceleration transmissibility of the floor when the dynamic vibration absorber is installed at different positions
(μ=0.1, λ=0.95, ζ=0.061)

The transmissiblity results are shown in Fig. 8(b). When the DVA is installed at the maximum mode shape, the reduction performance is greatest and the magnitude of the transmissibility is lower than other positions over the 30-40 Hz frequency band. when the absorber is moved away gradually from this position, the benefit reduces gradually. At the positions 0.5*L* and 0.25*L* is not affected by the DVA. It should also be mentioned that although the location of the output point will influence the benefit achievable from the DVA, the maximum benefit is still achieved when the DVA is located at the maximum of the mode shape. The ride comfort index calculation is conducted as well and the results can be found in Appendix. B. it shows a similar trand as the transimissibility results: the value is lowest when the DVA attached at the maximum modeshpe. And even if the application of DVA generate 2 peaks on curves,

the index will continue decreasing. Therefore, the position of each DVA is supposed to be close to the maximum of the mode shape.

5.2.2 Influence of the number of DVAs

In practice a single vibration absorber with a large mass and a large structure may not be allowed on the main structure due to practical limitations, so adding several absorbers with smaller mass at several suitable positions can be considered.

To study the effect of the number of absorbers, it is assumed that the total mass of the absorbers is kept as 0.16 kg. They are applied at the maximum point of the mode shape. After numerical calculation, for μ=0.1, the optimum parameters are found as λ=0.95-1.1, ζ=0.0058-0.061. Fig. 9(a) presents the variation of transmissibility with various number of absorbers, when the overall mass ratio is 0.01. The transmissibility gradually reduces as the number increases. The maximum value of transmissibility between 30 and 40 Hz is shown in Fig. 9(b) against the number of DVAs. The maximum value reduced by 36% when the number of DVAs is 2 compared with the case without DVA. When the number of absorbers is 4, the peak value is reduced by 40%, and the controlled frequency band is broadened. As it increased to 8, the peak value is reduced by 45%. when the number is greater than 4, the reduction of the floor vibration response is no longer sensitive to the number of DVAs. And the similar trend also can be found in the index calculation results.

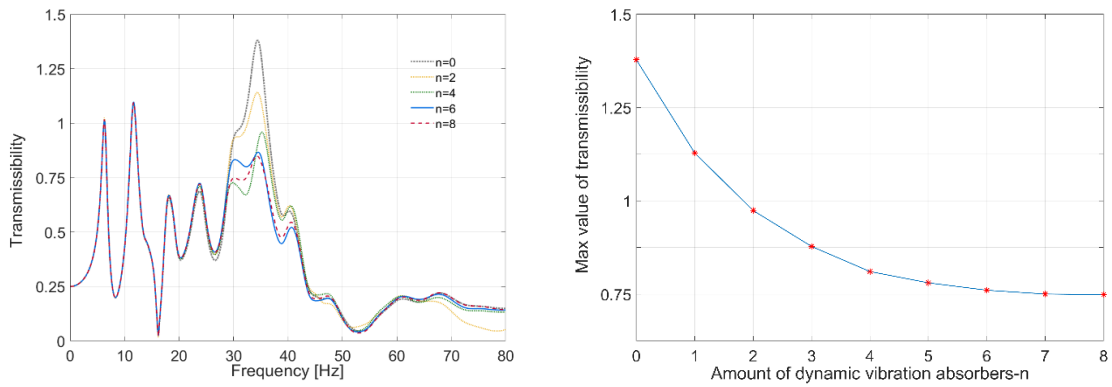

(a) acceleration vibration transmissibility (b) maximum value of transmissibility

Fig. 9 The effect of number of absorbers on acceleration vibration transmissibility and maximum value of transmissibility between 30 and 40 Hz (μ=0.1, λ=0.95-1.1, ζ=0.0058-0.061)

5.2.3 Influence of the mass ratio

Limited by the lighten design and installation space in the vehicle, the mass of the DVAs cannot increase infinitely. In this section the effect of mass ratio is studied while the natural frequency, position and damping ratio are constant.

Using the optimizing method in Eq.(17), the parameters of each DVA are obtained. Fig. 10(a) shows the transmissibility for different mass ratios. As the mass ratio increased, the maximum transmissibility around 30-40 Hz gradually decreased. For mass ratios greater than 0.04, the peak value is approximately unchanged, even if the mass ratio is increased further. Similar trends are also found for different numbers of absorbers. Fig. 10(b) presents the maximum transmissibility against the mass ratio for the system with 1, 2, 4 and 6 DVAs. In each case, for higher mass ratios, there is a decreasing trend, but the rate of reduction reduces. For the ride comfort index, the power from

mass ratio is not effective when the ratio is lower than 0.1 and the amount of DVA is 1. But the influence of mass ratio becomes effective while the amount is four, which can also be found in Appendix. B.

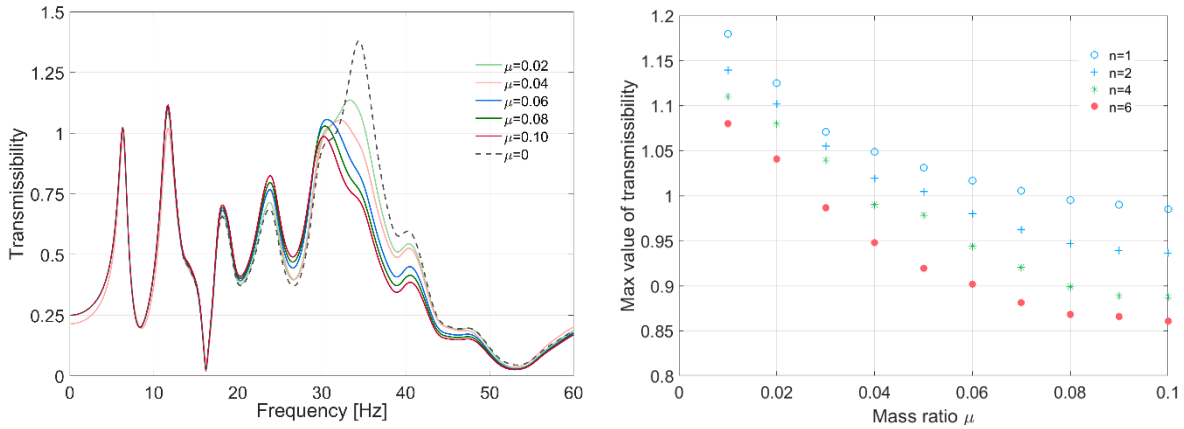

(a) Influence of mass ratio on transmissibility (b) maximum value of transmissibility

Fig. 10 The influence of mass ratio on transmissibility for a single DVA and maximum value of transmissibility for different numbers of DVA (μ=0.01-0.1, λ=0.95, ζ=0.0058-0.061)

5.2.4 Chosen configuration

In summary, for the design of the MDVAs controlling interior floor vibration in the high-speed EMU, each absorber needs to be installed close to the position of the maximum of the mode shape. Using a large number will bring a wider frequency control range. As the mass ratio is increased, the vibration attenuation effect is also improved, but the total mass of the system is also increased, so the additional performance of the absorbers is no longer obvious.

Tab. 2 Parameters of MDVAs for a high speed EMU

$\omega_c/2\pi$ (Hz)	n	$\omega_d/2\pi$ (Hz)	μ_i	m_i (kg)	k_i (N/m)	ζ
12.5	1	12.03	0.08	2068.1	10152	0.16
33.6	4	31.12	0.1	4	160.78	0.012
		32.58	0.1	4	176.18	0.012
		34.23	0.1	4	194.49	0.013
		35.30	0.1	4	206.85	0.019

According to the above discussion, the choice of DVA arrangement depends not only on the optimized parameters but also the situation in practice. In this study, the overall mass ratio for the mode at 33.6 Hz is selected as 0.04 and the number of absorbers is 4 to avoid excessive occupancy of the space under the interior floor. The mode at 12.5 Hz is controlled by a single DVA as discussed in section 5.1. The parameters finally chosen for each vibration absorber are shown in Tab. 2. The result of applying this combination of DVAs is shown in Fig. 11. The peak of the transmissibility in the region 30-40 Hz drops significantly, by about 33%.

For the realistic implementation of DVA, it is suggested that the lower frequency resonant needs a heavy mass can be suppressed with an underframe equipment and the DVA linked to the interior floor requires extra mass elements for a higher frequency flexural vibration such as 33.6 Hz, which be attached between the interior floor and structural floor next to the bus slot.

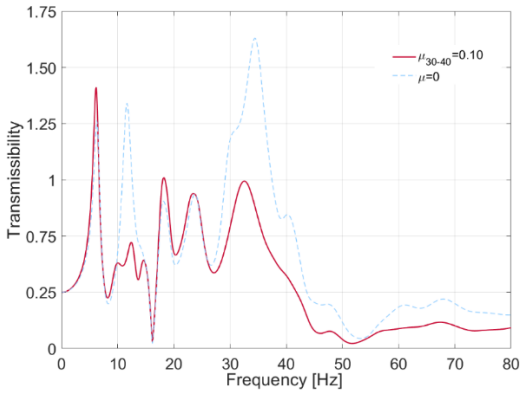

Fig. 11: The transmissibility of acceleration in the middle of the floor with dynamic absorbers at 12.5 and 33.6 Hz

5.3 Performance under realistic excitation

The DVAs with parameters listed in Tab. 2 are introduced into the refined simulation model with composite floor shown in Fig. 3. The vibration spectrum of the interior floor at the centre was evaluated to verify the design of the MDVAs. For comparison, the results without MDVA were also evaluated. During the investigation of local resonant, the input signal under the structural was collected by arranging accelerometers next to air springs sampling frequency of 1024 Hz. Then the collected signal is transferred in the FEA simulation as the excitation of the entire carbody at air springs as the measured vehicle.

The vibration acceleration spectra of the interior floor at the centre are shown in Fig. 12(a) , it can be observed that both the single DVA at 12.5 Hz and the MDVAs around 30-40 Hz effectively reduce the vibration of their control targets. To compare the effect on passenger's feeling, the vertical ride comfort evaluation method specified in the UIC 513 standard [1] is calculated. Fig. 12(b) shows the variation of UIC comfort index when the MDVAs are used to control different modes. The initial comfort index in the middle of the interior floor is over 2.5, indicating that the ride is only moderately comfortable. When DVAs with a mass ratio of 0.1 are connected to the interior floor, the vertical ride comfort index drops below 2.3. The variation of the index with different forms of absorbers is also showed in Fig. 12.

As the mass ratio increases, the index reduces in each case. However, the influence of the DVA at 33.6 Hz is smaller than for the single DVA at 12.5 Hz. This because the mode at 12.5 Hz made a large contribution to the comfort index, which can be seen from the limited change of comfort value when the MDVAs are mounted alone. When the DVAs at 12.5 Hz and 33.6 Hz are combined together the index is lower than for the DVA at 12.5 Hz alone. For the MDVAs at 33.6 Hz, the comfort index is gradually decrease as the increment of the mass ratio. The final effect of the multiple DVAs depends on the mass ratio and amount final selected.

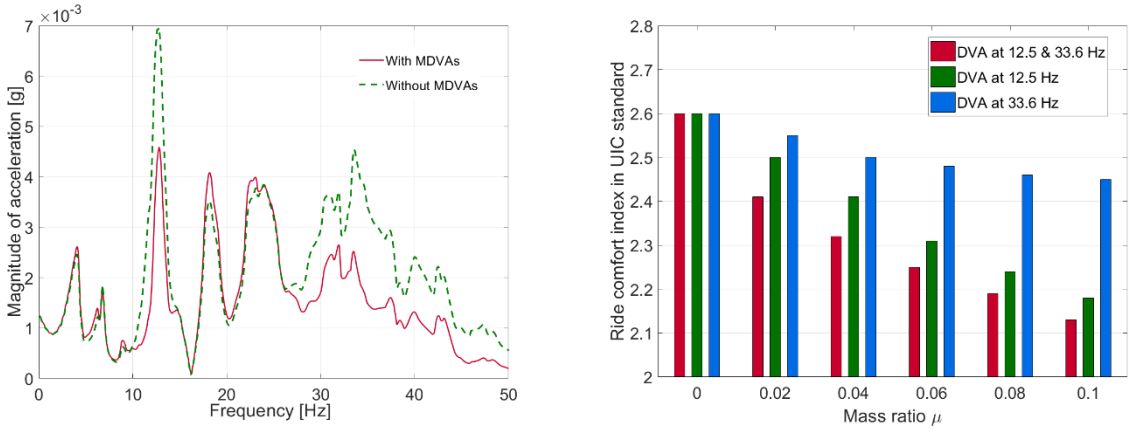

Fig. 12 (a) Comparison of simulated response in the middle of the floor in frequency domain

(b) Comparison of comfort index in the middle of the floor after introducing the dynamic vibration absorbers

6 Conclusions

The present study was designed to determine the effect of applying DVAs to reduce the local vibration of the interior floor of a high-speed train. With the help of measurements and a suitable model, the causes of the high local vibration are found to be the lack of local stiffness and inappropriate design of interior floor leading to a reduction of comfort for passengers. Based on this study, the following conclusions can be drawn:

1. It is found that a strong peak at around 12 Hz is dominated by a single mode of the whole carbody, which can be attenuated by using a single DVA. As this is a mode of the whole car body, the DVA can also be applied outside the car body, for example using under-floor equipment. For 30 and 35 Hz several local modes contribute to the high vibration levels, the vibration can be controlled by multiple DVAs. Methods are studied to determine the optimal parameters for these DVAs, including location, natural frequency and mass.
2. A floor vibration model and target mode identification method have been proposed for determining optimal parameters of multiple DVAs and the optimal design of the mass ratio and number of DVAs. The procedure is applied in a FEM model of the train structure. It yields the design and placement of the combination of DVAs that achieve suitable reduction in the peak response.
3. Five design parameters have been introduced to facilitate the optimization process. They are based on the maximum mode shape or the output point. Locating the DVA at the position at which the mode shape is maximum produced the most reduction and is recommended for practical applications.
4. It is found that four DVAs are sufficient to control the vibration of the interior floor structure. This number is linked to the number of modes that are active in the target frequency range. Increasing the number (for the same overall mass) does not appear advantageous.
5. The vibration at 30-40 Hz can also be improved by applying a damped floor (or a damped layer), but the damping is sensitive to the temperature, frequency and pressure, so a further research is needed in the future.

The approach used in the present work is not limited to the specific case of an interior floor. By modelling the host structure using FEA, based on modal expansion, the response of the whole structure can be decoupled into a set of discrete modal equations to which equations for the DVAs are added. This allows efficient optimisation of the properties of the DVAs applied to any structure.

Acknowledgments

The authors acknowledge the financial help provided by the Ministry of Science and Technology under the National Science and Technology Support Program project (Grant No. 2015BAG19B02 and 2015BAG13B01).

Appendix. A mathematical operation for transmissibility under *j*-th mode

The interior floor considered multiple DVAs and again assuming harmonic motion can be rewritten for a single mode as

$$-\omega^2\mathbf{M}_j\begin{Bmatrix}\mathbf{u}_j\\ \mathbf{Z}\end{Bmatrix}+i\omega\,\mathbf{C}_j\begin{Bmatrix}\mathbf{u}_j\\ \mathbf{Z}\end{Bmatrix}+\mathbf{K}_j\begin{Bmatrix}\mathbf{u}_j\\ \mathbf{Z}\end{Bmatrix}=\begin{Bmatrix}P\varphi_j(\mathbf{x_0})\\ \{0\}\end{Bmatrix} \tag{A1}$$

where

$$\mathbf{M}_j=\begin{bmatrix}M_j & & & \\ & m_1 & & \\ & & \ddots & \\ & & & m_N\end{bmatrix} \tag{A2}$$

$$\mathbf{C}_j=\begin{bmatrix}C_j+\sum_{n=1}^{N}c_n\varphi_j^2(\mathbf{x}_n) & c_1\varphi_j(\mathbf{x}_1) & \cdots & c_N\varphi_j(\mathbf{x}_n)\\ c_1\varphi_j(\mathbf{x}_1) & c_1 & 0 & 0\\ \vdots & 0 & \ddots & 0\\ c_N\varphi_j(\mathbf{x}_n) & 0 & 0 & c_N\end{bmatrix} \tag{A3}$$

$$\mathbf{K}_j=\begin{bmatrix}K_j+\sum_{n=1}^{N}k_n\varphi_j^2(\mathbf{x}_n) & k_1\varphi_j(\mathbf{x}_1) & \cdots & k_N\varphi_j(\mathbf{x}_n)\\ k_1\varphi_j(\mathbf{x}_1) & k_1 & 0 & 0\\ \vdots & 0 & \ddots & 0\\ k_N\varphi_j(\mathbf{x}_n) & 0 & 0 & k_N\end{bmatrix} \tag{A4}$$

The steady-state solution of Eq. (A1) the DVA responses can be written in the form:

$$\mathbf{Z}=Z_{\text{ref}}[s_{1,r}\ \ s_{2,r}\cdots s_{n,r}\cdots s_{N,r}]^T \tag{A5}$$

where $s_{n,r}=\varphi_j(\mathbf{x}_n)$, and Z_{ref} is a reference value for the vibration displacement amplitude. Substituting Eq. (A5) into Eq. (A1),

$$(-\omega^2\mathbf{M}_j+i\omega\,\mathbf{C}_j+\mathbf{K}_j)\mathbf{S}\begin{Bmatrix}\mathbf{u}_j\\ Z_{\text{ref}}\end{Bmatrix}=\begin{Bmatrix}P\varphi_j(\mathbf{x}_0)\\ \{0\}\end{Bmatrix} \tag{A6}$$

where

$$\mathbf{S}=\begin{bmatrix}1 & 0\\ 0 & s_{1,r}\\ \vdots & \vdots\\ 0 & s_{M,r}\end{bmatrix} \tag{A7}$$

When the *j*-th mode is dominate, the response of the structure is:

$$\mathrm{u} = \mathrm{W}\, e^{iwt} \tag{A8}$$

Then the vibration of the structure can be obtained by solving Eq. (A6)

$$W_j = \frac{\varphi_j(\mathbf{x}_0) P}{M_j \omega^2 - K_j + \sum_{n=1}^{N} \frac{m_n \varphi_j^2(\mathbf{x}_n)\, \omega^2 (i\omega c_\mathrm{n} + k_\mathrm{n})}{-\omega^2 m_\mathrm{n} + i\omega c_\mathrm{n} + k_\mathrm{n}}} \tag{A9}$$

To simplify the expressions, the following terms are introduced:

$$\mu_{jn} = m_n / M_j \quad \lambda_j = \omega/\omega_j \quad \gamma_{jn} = \omega_n/\omega_j \quad \zeta_n = c_n/(2m_n\omega_n) \quad \delta_{st,j} = P/K_j \tag{A10}$$

where μ_{jn} is the mass ratio of *n*-th DVAs, λ_j is the ratio of the forcing frequency ω to the modal frequency ω_j, γ_{jn} is the ratio of the natural frequency ω_n of *n*-th DVAs to that of the structural mode ω_j, ζ_n and $\delta_{st,j}$ is a generalized displacement amplitude and *P* is the amplitude of the harmonic force.
Substituting to Eq. (A9) for displacement and acceleration, results in:

$$|W_j| = \frac{|\varphi_j(\mathbf{x}_0)|\omega_j^2}{-\omega^2\sqrt{\mathrm{Re}^2 + \mathrm{Im}^2}} \tag{A11}$$

$$\left|\ddot{W}_j\right| = \frac{|\varphi_j(\mathbf{x}_0)|\omega_j^2}{\sqrt{\mathrm{Re}^2 + \mathrm{Im}^2}} \tag{A12}$$

Where

$$\mathrm{Re} = 1 - \frac{1}{\lambda_j^2} + \sum_{n=1}^{\mathrm{N}} \frac{\mu_{jn}\varphi_j^2(\mathbf{x}_n)[(1-\lambda_j^2/\gamma_{jn}^2)^2 + (2\zeta_n\lambda_j/\gamma_{jn})^2]}{(1-\lambda_j^2/\gamma_{jn}^2)^2 + (2\zeta_n\lambda_j/\gamma_{jn})^2} \tag{A13}$$

$$\mathrm{Im} = \sum_{n=1}^{\mathrm{N}} \frac{\mu_{jn}\varphi_j^2(x_n, y_n)(2\zeta_n\lambda_j^3/\gamma_{jn}^3)}{(1-\lambda_j^2/\gamma_{jn}^2)^2 + (2\zeta_n\lambda_j/\gamma_{jn})^2} \tag{A14}$$

And the transmissibility can be shown as:

$$T = \left|\frac{\ddot{W}_j}{\delta_{st,j}}\right| = \sqrt{\frac{\varphi_j(\mathbf{x}_0)^2\omega_j^4(\lambda_j^2)^2[(\gamma^2-\lambda_j^2)^2 + (2\zeta\lambda_j)^2]}{[(1-\lambda_j^2)(\gamma^2-\lambda_j^2) - A\gamma^2\lambda_j^2]^2 + [1-(1+A)^2\lambda_j^2]^2(2\zeta\lambda_j)^2}} \tag{A15}$$

where

$$A = \mu\left(\sum_{n=1}^{N} \boldsymbol{\varphi}_j^2(\mathbf{x}_n)\right) \tag{A16}$$

According to the fixed-point theory, there will be two points which are nonrelated to the damping of the system and it is defined an optimal modem process when the points are with the same peaks value.
When the damping ratio ζ=0, the transmissibility can be express as:

$$\left|\frac{\ddot{W}_j}{\delta_{\mathrm{st},j}}\right| = \frac{|\varphi_j(\mathbf{x}_0)|\omega_j^2\lambda_j^2(\gamma^2-\lambda_j^2)}{(1-\lambda_j^2)(\gamma^2-\lambda_j^2) - A\gamma^2\lambda_j^2} \tag{A17}$$

When the damping ratio ζ=∞, the transmissibility can be express as:

$$\left|\frac{\ddot{W}_j}{\delta_{\mathrm{st},j}}\right| = \frac{\varphi_j(\mathbf{x}_0)\,\omega_j^2\lambda_j^2}{1-\lambda_j^2(1+A)} \tag{A18}$$

The cross point of these two curves can be solved as:

$$\frac{|\varphi_j(\mathbf{x}_0)|\omega_j^2\lambda_j^2(\gamma^2-\lambda_j^2)}{(1-\lambda_j^2)(\gamma^2-\lambda_j^2)-A\gamma^2\lambda_j^2} = \frac{\varphi_j(\mathbf{x}_0)\,\omega_j^2\lambda_j^2}{1-\lambda_j^2(1+A)} \tag{A19}$$

Supposing the solutions of Eq. (A19) are λp and λq, substituting to Eq. (A19):

$$\frac{\varphi_j(\mathbf{x}_0)\,\omega_j^2\lambda_p^2}{1-\lambda_p^2(1+A)} = -\frac{\varphi_j(\mathbf{x}_0)\,\omega_j^2\lambda_q^2}{1-\lambda_q^2(1+A)} \tag{A20}$$

$$\lambda_p^2\lambda_q^2 = \frac{2\gamma^2}{2+A} \tag{A21}$$

Solving simultaneous Equations of (A20) and (A21)

$$\lambda_p^2+\lambda_q^2 = \frac{2+2\gamma^2(1+A)}{2+A} = 2(1+A)\frac{2\gamma^2}{2+A} \tag{A22}$$

Then the tuned-frequency ratio can be expressed as:

$$\gamma_{op} = \frac{1}{1+A} \tag{A23}$$

Substituting Eq. (A23) to Eq. (A19), the optimal damping ratio is:

$$\zeta_{op} = \sqrt{\frac{3A}{8(1+A)^3}} \tag{A24}$$

Appendix. B Ride comfort index results for different research session

Tab. B1 Ride comfort index results for different research session

Session	Type	Ride comfort index					
Placements μ=0.1	0 L	2.60					
	0.25 L	2.60					
	0.50 L	2.60					
	0.75 L	2.60					
	1 L	2.58					
Number μ=0.1	0	2.60					
	2	2.57					
	4	2.56					
	6	2.56					
	8	2.56					
Mass ratio		μ=0	μ=0.02	μ=0.04	μ=0.06	μ=0.08	μ=0.1
	n=1	2.60	2.60	2.60	2.59	2.59	2.58
	n=4	2.60	2.55	2.5	2.48	2.46	2.45

References

[1]. UIC Code 513. Guideline for evaluation passenger comfort relation to vibration in railway vehicles. Paris: International Union of Railways (UIC) & European Committee for Standard (CEN), 1994.

[2]. ISO 2631-1. Mechanical vibration and shock – evaluation of human exposure to whole-body vibration – part 1: general requirements, Switzerland, 1997.

[3]. Takahiro Tomioka, Takigami, Tadao. Reduction of bending vibration in railway vehicle carbodies using carbody-bogie dynamic interaction. Vehicle System Dynamics, 2011, 49(5):831-831.

[4]. Lai Wei, Jing Zeng, Maoru Chi & Jianbin Wang (2017) Carbody elastic vibrations of high-speed vehicles caused by bogie hunting instability, Vehicle System Dynamics, 55:9, 1321-1342

[5]. J. L. Escalona, H. Sugiyama & A. A. Shabana (2013) Modelling of structural flexibility in multibody railroad vehicle systems, Vehicle System Dynamics, 51:7, 1027-1058

[6]. Graa, M., et al. Development of a reduced dynamic model for comfort evaluation of rail vehicle systems. Proceedings of the Institution of Mechanical Engineers, Part K: Journal of Multi-body Dynamics 230.4 (2016): 489-504.

[7]. J.S. Zhou, R. Goodall, L. Ren, etal., Influences of carbody vertical flexibility on ride quality of passenger railway vehicles, Proc. IMech E Part F: J. Rail Rapid Transit 223(2009);461–471.

[8]. Foo E, Goodall R M. Active suspension control of flexible-bodied railway vehicles using electro-hydraulic and electro-magnetic actuators .Control Engineering Practice, 2000, 8(5):507-518.

[9]. Carlbom P. Combining MBS with FEM for rail vehicle dynamics analysis. Multibody System Dynamic 2001; 6: 291–300

[10]. Dao Gong, Jinsong Zhou, Wenjing Sun et al. Method of multi-mode vibration control for the carbody of high-speed electric multiple unit trains，Journal of Sound and Vibration, 2017,409, 94-111.

[11]. Tomioka, T., Y. Suzuki and T. Takigami, Three-dimensional Flexural Vibration of Lightweight Railway Vehicle Carbody and a New Analytical Method for Flexural Vibration. Quarterly Report of RTRI, 2003. 44(1): 15-21

[12]. Wang, Z. and C.M. Mak, Application of a movable active vibration control system on a floating raft. Journal of Sound and Vibration, 2018. 414: 233-244.

[13]. Yayun Qi, Huanyun Dai, Chunyuan Song, Sheng Qu. (2019) Shaking analysis of high-speed train's carbody when cross lines. Journal of Mechanical Science and Technology 33:3, 1055-1064.

[14]. Gong, Dao, et al. Car body floor vibration of high-speed railway vehicles and its reduction. Journal of Low Frequency Noise, Vibration and Active Control (2019): 1461348419850921.

[15]. Hudson C, Carruthers J and Robinson A. Multiple objective optimisation of composite sandwich structures for rail vehicle floor panels. Composite Structures 2010; 92: 2077–2082.

[16]. Takigami T, Tomioka T and Aida K. Improving the rigidity of railway vehicle carbodies using non-structural members. QR RTRI 2009; 50: 63–69.

[17]. J. Ormondroyd, J.P. Den Hartog, The theory of the dynamic vibration absorber, Transactions of the American Society of Mechanical Engineers 50 (1928) A9–A22.

[18]. R. G. Jacquot. Suppression of Random Vibration in Plates Using Vibration Absorbers. Journal of Sound and Vibration, 2001, 248(4): 585-596

[19]. Van Niekerk, J. L., Pielemeier, W. J., & Greenberg, J. A. The use of seat effective amplitude transmissibility (SEAT) values to predict dynamic seat comfort. Journal of sound and vibration. 2003,260(5), 867-888.

[20]. J.P. Den Hartog, Mechanical Vibrations, Dover Publications, New York, 1985.

[21]. J.B. Hunt, Dynamic Vibration Absorbers, Mechanical Engineering Publications, London, 1979.

[22]. Nguyen, T. H., et al. Performance of distributed multiple viscoelastic tuned mass dampers for floor vibration applications. Advances in Structural Engineering 15.3 (2012): 547-562.

[23]. Zhu, S., Yang, J., Yan, H., Zhang, L., & Cai, C. (2015). Low-frequency vibration control of floating slab tracks using dynamic vibration absorbers. Vehicle System Dynamics, 53(9), 1296-1314.

[24]. Collette C, Horodinca M, Preumont A. Rotational vibration absorber for the mitigation of rail rutting corrugation. Vehicle System Dynamics. 2009, 47(6): 641-659

[25]. Chen Z, Fang H, Han Z, et al. Influence of bridge-based designed TMD on running trains. Journal of Vibration & Control.2019;25:182–193.

[26]. Gong, Dao, J. S. Zhou, and W. J. Sun. On the resonant vibration of a flexible railway car body and its suppression with a dynamic vibration absorber. Journal of Vibration & Control 19.5(2013):649-657.

[27]. Griffin, M.J. Handbook of human vibration. Academic press, 2012

[28]. Ewins, D. J. Modal testing: theory, practice and application, second edition, 2000. Research Studies Press, Baldock, Hertfordshire, England, 171, 415-437.
[29]. Park J, Ha T, Kim H. Finite element modelling and experimental verification of lightweight steel floor vibration. Journal of Vibration Engineering. 2016, 18(3): 1435-1443.
[30]. Tedesco, Joseph, William G. McDougal, and C. Allen Ross. Structural dynamics. New York: Pearson Education, 2000.
[31]. Esfandiari, A., Bakhtiari-Nejad, F., Rahai, A., & Sanayei, M. (2009). Structural model updating using frequency response function and quasi-linear sensitivity equation. Journal of Sound and Vibration, 326(3-5), 557-573.
[32]. Nieto, M., Elsayed, M., & Walch, D. (2018). Modal Participation Factors and their Potential Applications in Aerospace: A Review.
[33]. Kim, Sung-Yong, and Cheol-Ho Lee. Optimum design of linear multiple tuned mass dampers subjected to white-noise base acceleration considering practical configurations. Engineering Structures 171 (2018): 516-528.
[34]. Xia Z, Zhou J, Liang J, et al. Online detection and control of car body low-frequency swaying in railway vehicles. Vehicle System Dynamics. 2019, 1: 1-31.
[35]. Wei Sun, Xianfei Yan & Feng Gao. Analysis of frequency-domain vibration response of thin plate attached with viscoelastic free layer damping, Mechanics Based Design of Structures and Machines, 2018, 46:2, 209-224.